

1 Quantifying vein attributes in massive mudstones (Triassic, SW
2 England): implications for progressive evolution of opening-
3 mode fracture networks

4 **Qingfeng Meng, John N. Hooker, and Joe Cartwright**

5 *Department of Earth Sciences, University of Oxford, South Parks Road, Oxford, OX1 3AN, UK*

6 Email: meng.qingfeng@hotmail.com

7 **ABSTRACT**

8 Attributes of gypsum vein arrays in the Triassic massive mudstones of SW England were analyzed
9 to infer the process of vein network evolution. Field data demonstrate that there is no clear
10 correlation between vein orientation and thickness; however, sub-horizontal veins have a higher
11 average thickness than the inclined veins. Vein thickness distribution is best characterized by a
12 log-normal distribution. The fractal dimensions ' D ' of vein networks analyzed range from 1.44 to
13 1.71. Vein networks, which contain abundant bridging veins between neighbouring sub-horizontal
14 veins to form an anastomosing pattern, exhibit a higher D value. The fraction of vein volume
15 derived from image analysis ranges from 6.75 to 17.94%. A positive correlation is revealed by
16 plotting the fractal dimensions of the vein networks versus the number of vein-intersection points,
17 suggesting that an anti-clustering distribution of veins could contribute to more interactions and
18 also intersections of the gypsum veins. The vein attribute data presented indicate that
19 mineralization in the massive mudstones is mainly localized to some of the largest veins as a result

of mechanical interaction of neighbouring veins during vein propagation, hindering the nucleation of new veins as a consequence. Accommodation of the bulk rock strain could be facilitated mainly by expansion of the large, backbone veins, which follow a positive feedback mechanism of growth. This study reveals a strong link between the geometric parameters of opening-mode fractures with the history of their formation, propagation and intersection.

Key words: log-normal; thickness distribution; fractal dimension; opening-mode fracture; vein

1. Introduction

Low-permeability mudstones largely rely on natural fractures, especially opening-mode fractures, as pathways for fluid flow (e.g. Aydin, 2000; Engelder et al., 2009; Meng et al., 2017a, b). Fracture systems can hence control the overall permeability and define the hydraulic properties of the rocks. The study of natural fracture systems in mudstones has been an active area motivated to a large extent by induced hydraulic fractures during shale gas stimulation in recent years (e.g. Curtis, 2002; Gale et al., 2007; Engelder et al., 2009; Cobbold et al., 2013; Gale et al., 2014; Hooker et al., 2017). The difficulty in understanding opening-mode fractures is that they could arrest or even heal, when the fluid pressure in the fractures drops during fracture propagation (Renshaw and Harvey, 1994; Cosgrove, 2001; French et al., 2012). However, the characteristics of opening-mode fractures can be well-preserved if the fractures have been cemented by mineral aggregates precipitated from focused fluid flow in fracture channels. Mineral veins, as a record of fluid circulation and an increase of rock permeability, can yield insights into the formation of fractures and also fluid-rock interactions (Passchier and Trouw, 1996; Oliver and Bons, 2001; Bons et al., 2012).

Several geometric attributes have been used to characterize mineral veins, mainly including size (length, thickness and length/thickness ratio) and size distribution (e.g. Clark et al., 1995; Bonnet

et al., 2001; Olson, 2003; Hooker et al., 2009, 2012, 2014; Guerriero et al., 2010), spacing (e.g. Narr and Suppe, 1991; Rives et al., 1992; Bai et al., 2000; Guerriero et al., 2011; Hooker and Katz, 2015; Hooker et al., 2018), fractal analysis of fracture traces (e.g. Walsh and Watterson, 1993; McCaffrey and Johnston, 1996; Roberts et al., 1998), connectivity (e.g. Berkowitz et al., 2000; Darcel et al., 2003; Ghosh and Mitra, 2009), paleo-fracture porosity (defined as $\text{Area}_{\text{vein}} / \text{Area}_{\text{rock}}$ in a two-dimensional sampling domain) (e.g. Narr and Currie, 1982; Hood et al., 2003; Laubach et al., 2004; Gale et al., 2010). Statistical analysis of these parameters provides insights into how the vein geometric patterns arise and their potential significance for reconstructing the history of vein network development.

This paper presents a study of a mineralized fracture network of the poorly bedded Mercia Mudstone (Late Triassic) outcropping in SW England. We first describe multiple vein attributes, including thickness, thickness distribution, intersection, fractal dimension and vein volume fraction, then discuss their geological implications. Finally, a conceptual model is proposed to explain the formation and evolution of the vein networks. The aim of this paper is to use coupled vein attribute data to infer the process of formation of an anastomosing, opening-mode fracture network. This study highlights the importance of mechanical interaction and coalescence of veins during propagation, which may exert strong controls on localized mineralization in the rock matrix. The thickness distribution of the vein arrays and the positive feedback growth mechanism proposed can be instructive for subsurface fracture prediction and numerical modeling of opening-mode fracture network development in massive low-permeability rocks.

2. The Mercia Mudstone

The Triassic Mercia Mudstone Group in this study is located at the Warren Bay, near Watchet, north Somerset, UK (Fig. 1), where the Triassic Mercia Mudstone Group is exposed in the 1.5 km long, E-W-striking cliffs. The Mercia Mudstone outcrops in a horst that is bounded to the south by the E-W-striking Helwell Bay Fault (Meng et al., 2017). The Helwell Bay Fault and numerous E-W-striking, outcrop-transecting faults are suggested to develop initially as normal faults during extension and subsidence of the Bristol Channel Basin through the Triassic and Jurassic (Miliorizos and Ruffell, 1998). Those faults have reactivated in the Early Cenozoic as a result of N-S compression due to the Alpine Orogeny (Van Hoorn, 1987; Brooks et al., 1988; Kelly et al., 1999; Glen et al., 2005). Many reverse-reactivated normal faults retain finite normal displacements; however, some faults changed into reverse faults (Dart et al., 1995).

The Mercia Mudstone exposed in the study area consists of dominantly red, less commonly green-grey, unfossiliferous marls and subordinate siltstones, which are massive (unstratified) and lacking apparent laminations. The striking feature of the red marls in the Watchet area is that they contain several beds of nodular gypsum masses, which formed in hypersaline and evaporitic mudflats in the environment of sabkha (Taylor, 1983; Warrington and Ivimey-Cook, 1992; Hobbs et al., 2002; Howard et al., 2008). Gypsum is also present as whitish, opaque veins (Cosgrove, 2001; Philipp, 2008; Meng et al., 2017b, c). The veins commonly consist of a median zone of red host rock inclusions and parallel-aligned, fibrous gypsum crystals that are normal or partly oblique to vein walls. The gypsum veins are mostly sub-horizontal, whilst steeply dipping veins are also abundant in some beds, including many NW-SE striking, north dipping veins and E-W-striking, south dipping veins. Differently oriented veins exhibit an overall anastomosed vein pattern.

3. Methodology

Vein orientation and thickness data were measured in the field to examine the control of vein orientation on thickness. To gather thickness distribution data, we selected seven sites along the sub-vertical cliffs in the study area, where the gypsum veins exhibit a complex pattern. All vein thicknesses were collected within circular windows with a diameter of 0.5*0.5 m for closely-spaced (<5cm) vein arrays, or 1*1 m for more sparsely-spaced vein arrays. Compared to linear scanline sampling methods, the circular window method offers a more efficient sampling tool for characterizing the geometry of fracture (vein) traces, and can gather information of veins exhibiting varied patterns within different horizons in 2D (Mauldon et al., 2001; Rohrbaugh Jr et al., 2002). To reduce the sampling bias due to undersampling the smallest veins, a vein-thickness comparator (Ortega et al., 2006) was used to measure the thickest parts of veins, with a lowest detection limit of 0.1 mm. One data point of thickness was gathered for each vein. Each sampling site contains at least 50 veins, which could ensure a valid statistical analysis at a confidence level of 86% (Priest and Hudson, 1976). Vein thickness data were analyzed by scatter plot of vein-thickness versus cumulative frequency. The resulting curves were fit with power-law, exponential, normal and log-normal equations (Hooker et al., 2012, 2013, 2014). A chi-squared test is applied to determine whether there is a significant difference between the expected frequencies and the observed frequencies, where the lowest χ^2 error values indicate the best fit thickness distribution.

The study on vein intersections, fractal dimension and vein volume fraction was conducted by image analysis of high-resolution field photos (see supplementary material). Vein volume fraction is here defined as ratio of total area of vein sections versus the total area of the host rock section (0.5*0.5 m). The photos show 2D vein arrays which exhibit different geometries and interactions. The red marls and white gypsum veins show a clear contrast in color in these photos, which permits identification and mapping of vein networks. The number of intersection points in the vein

networks were counted at higher resolutions to show great details of vein traces. The contrast of the images were enhanced and then transformed to binary images by assigning black color to gypsum veins and white color to the host marls. A manual modification of the automatically generated binary images was conducted by comparing those images to the original images to improve the quality of vein recognition. Vein volume fraction data was obtained using Photoshop software by calculating the ratios of black-pixel number versus the number of all pixels the image contains.

Fractal dimension ' D ' of fractures (veins), as a measure of spatial occupancy of the fracture network, was used to characterize the local variation in complexity of fracture distribution by a box-counting method (e.g. Gillespie et al., 1993; Walsh and Watterson, 1993; Bonnet et al., 2001). The images analyzed were divided into numerous boxes with an equal area and a side length of ε . The number of boxes $N(\varepsilon)$ that contain veins were counted. D can then be calculated by regression analysis of $\ln \varepsilon - \ln N(\varepsilon)$, which is determined by:

$$D = -\lim_{\varepsilon \rightarrow 0} \frac{\ln N(\varepsilon)}{\ln \varepsilon}$$

All D values are expected within the range $1 < D < 2$. We used ImageJ software for calculating the fractal dimension (Jafari and Babadagli, 2011; Karperien, 2013) of the gypsum vein networks. The parameters of vein attributes derived from image analysis, including number of vein intersection points, fractal dimension and fracture porosity, were then plotted to evaluate their mutual influences.

56 rock samples were cut to thin sections for making observations on microscopic features of gypsum veins and cements in the host marls. Elemental maps of the thin sections were produced

using scanning electron microscope (SEM) based energy-dispersive X-ray spectroscopy (EDS), in order to make observations of the geometry, texture and size of the gypsum crystals.

4. Results

4.1. Vein thickness and thickness distribution

The gypsum veins measured in the circular sampling sites have a range of thickness, extending up to nearly three orders of magnitude. The maximum thickness of single veins varies between 0.1 and 22 mm, with an average value of 2.3 mm. Veins with a thickness of 0.5 - 1.5 mm occupy the largest proportion (39.9%) in the total population. The plot of vein thickness versus orientation demonstrates that there is no clear correlation between them (Fig. 2). However, the average thickness of gently-dipping veins (dip < 30°) reaches 4.1 mm, which is higher than more steeply-dipping veins (1.89 mm). The thickest vein observed along the outcrop is 170 mm in thickness but was not sampled by a scanline. Veins, exceeding 100 mm in thickness, predominantly occur either as fault-filling veins or sub-horizontal veins.

The thickness distribution of the gypsum veins is best characterized by a log-normal distribution (Fig. 3), corroborated by the lowest χ^2 (Table 1). It is notable that some deviations from the expected log-normal trends occur, where vein thickness exceeds 10 mm. The actual population of thick veins (>10 mm) is higher than the value extrapolated from smaller fractures. It is likely that such deviations result from sampling bias due to undersampling of the smallest veins at sizes beneath the detection limit.

In thin sections microfractures with a thickness lower than 0.1 mm were rarely observed (Fig. 4A).

Minor veins, around 0.1 mm in thickness, exhibit similar elongate-fibrous texture to the

neighbouring macro sized veins (Fig. 4A, B). Lenticular gypsum crystals, commonly exhibiting tapering tips and random orientations, were found in the rock matrix (Fig. 4A, C). They occur either as isolated individuals or closely-packed aggregates, with a thickness as low as 5 μm . Unlike other minor veins and macro veins, such gypsum crystals are textureless, and are considered to be gypsum pseudomorphs after burial anhydrite-laths rather than microfractures (Shearman and Fuller, 1969; Chandler, 1988; Kasprzyk, 1995). Hence, the sizes of such gypsum crystals were not taken into account in the vein-thickness data sets.

4.2. Vein intersection

Mudstone units that only contain sub-horizontal gypsum veins do not exhibit a complex vein network geometry (Fig. 5). As vein intensity and connectivity increase, vein interactions occur, where vein tips coalesce with the tips or walls of their neighbouring veins (Fig. 6).

Vein intersections at low angles ($< 30^\circ$) commonly appear where a set of gently dipping en echelon veins link with neighbouring veins (Fig. 6A), resulting in linear segments of the host rock entrapped between the tips. Vein branching, i.e. where a single vein splits into two or multiple segments, with a sum of branch thickness approximately equal to the parent vein, commonly occurs during their lateral propagation (Meng et al., 2017b) (Fig. 6B). The branches and the parent vein often form intersections at low angles. Multiple sub-parallel veins with a spacing less than 10 cm commonly deviate from the original propagation direction gently and coalesce with adjacent veins, or split into thinner branches which also coalesce with the upper and lower neighbouring veins (Fig. 6C). Steeply-dipping veins are often observed to occur within the intervals between two sub-horizontal veins, with both ends intersecting with the walls of the sub-horizontal veins at an angle greater than 30° (Fig. 6D). Importantly, the steep, bridging veins in a complex vein

network contribute to an increased connectivity by linking sub-horizontal veins, with at least two vein intersections. Minor veins with tapering tips are observed to propagate towards the walls of larger veins (Fig. 6E). The intersection angles can reach up to nearly 90°. Some veins split into multiple braches, which propagate in an acute fashion to be orthogonal to the walls of a neighbouring, larger vein, and coalesce with the vein wall by tip-wall intersections (Fig. 6F). Hence, the density of intersection points increases dramatically in the zones where veins approach others.

The result of image analysis demonstrates that the vein networks containing a lower amount of intersection points mainly consist of sub-horizontal veins (Fig. 7A, B) (Table 2), whereas those with more intersection points have more abundant steep, bridging veins (Fig. 7C, D).

4.3. Fractal dimension

The fractal dimensions ' D ' of vein networks analyzed range from 1.44 to 1.71 (Table 2), with an average value of 1.61. The vein network having the lowest D mainly consists of sub-horizontal veins, especially en echelon vein sets (Fig. 7A, B). Tapering, sharp vein tips are commonly identifiable, which are not linked with adjacent veins. Steeply-dipping veins are mainly clustered within a few units, whereas the rest of the rock volume is not fractured and contains few veins. In contrast, vein arrays with a higher D exhibit much more complex geometries and patterns (Fig. 7C, D). There are a substantial number of inclined veins that transect the regions between two or more sets of sub-horizontal veins. Vein linkage and interaction are common between differently oriented veins, which makes it difficult to identify vein tip structures.

4.4. Vein volume fraction

Vein volume fraction, as demonstrated by image analysis (Fig. 7B, D), ranges from 6.75 to 17.94% (Table 2), with an average value of 11.24%. Because vein volume fraction is determined by the total area of the vein section, the measurement result can be higher than the actual value if the size-fixed circles capture too many thick veins as their dominant vein sets (Fig. 5C).

4.5. Relationship between fracture porosity, fractal dimension, and intersection

The plot of vein volume fraction versus the number of intersection points demonstrates that there is no clear correlation between them (Fig. 8A). This result indicates that less populated vein networks with fewer vein intersections may have an equal or even higher vein volume than the more complex vein networks with more vein intersections. Similarly, vein volume fraction and fractal dimension do not exhibit clear correlations. This indicates that the vein arrays may either be more clustered, or more homogeneously distributed, given a distinct vein volume fraction for a vein network.

A positive correlation is revealed from the plot of fractal dimension versus number of intersection points (Fig. 8B). This indicates that if the vein arrays filled the host rock matrix evenly, the veins would exhibit more interactions, and hence more intersections with adjacent veins. In this case, thickness of individual veins does not affect vein intersections and vein network connectivity.

5. Discussion

5.1 Origin of the vein thickness distribution

The thickness distributions of mineral veins can reflect the mechanisms responsible for the formation and evolution of the vein networks (Clark et al., 1995). In many previous studies, vein thickness (fracture aperture) distributions have generally been found to conform to power-law

distributions (e.g. Segall and Pollard, 1983; Gudmundsson, 1987; Marrett and Allmendinger, 1992; Sanderson et al., 1994; McCaffrey and Johnston, 1996; Ortega et al., 2006; Hooker et al., 2009, 2013, 2014). The power-law distribution implies a scale-free and self-similar vein (fracture) pattern, i.e., a pattern lacking a characteristic size, with sizes covering up to several orders of magnitude (Bonnet et al., 2001). The reason for power-law distributions versus other types of distributions still remains uncertain, although a number of models have been explored. It has been suggested that power-laws could occur in vein arrays characterized by vein dynamic interaction (e.g., linkage or coalescence) (Cowie et al., 1993; Clark et al., 1995; Cladouhos and Marrett, 1996; Davy et al., 2010; Hooker et al., 2012). Sampling effects imposed on a power-law population may cause the distribution to be better fit by a log-normal distribution (Bonnet et al., 2001). Because of the finite size of the sampled domain and the resolution limitations of the sampling technique, it is possible to under-sample the smallest veins resulting in a truncation effect, or to miss the largest veins that intersect the sampling area boundaries, or to exclude the very largest veins resulting in a censoring effect (Einstein and Baecher, 1983; Segall and Pollard, 1983; Bonnet et al., 2001). It has also been suggested that grain size can influence fracture density at micro-scale, thereby resulting in a vein thickness distribution diverging from a power law (Guerriero et al., 2013). The presence of a characteristic size scale, which is commonly provided by lithological layering, can often cause log-normal distributions (Odling et al., 1999).

In this study, the vein thickness is best fit by a log-normal distribution (Fig. 3), which could have resulted from the following two factors. Firstly, the vein thickness predominantly fall within the range of 0.1 mm to 10 cm, i.e. four orders of magnitude, which means any fractal-type scaling processes are active over only a limited size range. Secondly, the common coalescence of parallel veins during lateral propagation, especially en echelon veins, could reduce the number of small

veins and their relative proportion. The merged larger veins could also contribute to an increase in the number of larger veins. The dynamic changes in the relative proportions of small to large veins may then shift to a log-normal distribution as a consequence.

5.2 Vein growth and mechanical interaction

Three types of vein distribution were recognized in this study, including (1) isolated, sub-horizontal veins (Fig. 5A); (2) closely-spaced, sub-horizontal vein arrays (Fig. 5B, C); and (3) well-connected, dense vein networks (Figs 6E, F and 7). Our field observations demonstrate that the isolated sub-horizontal veins generally have the greatest thickness. Smaller and steeply-dipping veins are rarely observed in the horizons nearby, suggesting that such veins acted as the main fluid conduits in these beds, from which gypsum was precipitated onto vein surfaces.

As the density of the vein set increases, en echelon vein arrays commonly link with neighbouring veins, whilst vein coalescence between different horizons is rare. The thickness of small veins within the intervals of two neighbouring sub-horizontal veins is commonly below 1 mm, although the total vein volume can still be relatively high. This suggests that vein growth is largely localised to the thick, sub-horizontal veins. Such a growth localization has been suggested to result from mechanical interaction of the vein arrays as predicted by linear elastic fracture mechanics (Ingraffea, 1987; Renshaw and Harvey, 1994; Olson, 2003). The occurrence of large veins (thickness > 1cm) could reduce the tensile effective stress in the surrounding rocks perpendicular to the vein plane (Olson and Pollard, 1989; Rives et al., 1992), so that the growth of smaller veins may be inhibited. Large veins serve as the major fluid drains in the rock volume, which could affect the development of smaller veins around them, and thereby affect the thickness distribution characteristics (Roberts et al., 1998, 1999).

The characteristic feature of the vein networks with a high connectivity is that they exhibit a high fractal dimension and also a high fracture porosity. Because in poorly bedded successions the localized stress field has been suggested to be proportional to the vein length, larger veins generally have greater stress intensity and could subject more and more smaller veins into their stress shadows during propagation (Ingraffea, 1987). Smaller veins in such stress shadows tend to become clustered (Weertman et al., 1983; Olson, 1993). Meanwhile, the tip zones of large veins are regions of enhanced effective stress, which promotes the growth of smaller veins (Olson, 1993; Renshaw and Pollard, 1994). This is commonly evident from veins splitting into minor branches during their propagation (Fig. 6F). The well-connected vein networks, as a result of vein propagation and linkage, form a backbone in the host rock, where the transport of gypsum has been largely focused within the restricted part of the networks. This leads to gypsum precipitation mainly in the large, connected veins as backbones rather than the small, unconnected veins. As the vein population and connectivity grow, vein intensity continues to increase until no more veins can nucleate owing to the interaction of stress shadows, i.e. the ‘saturation level’ (Narr and Suppe, 1991; Rives et al., 1992; Bai and Pollard, 2000). At this stage, the strains developed in the bulk are mainly expressed by widening of pre-existing veins rather than the nucleation of new veins. The gypsum veins in the study area may possibly have approached the saturation level as evident from the lack of micro-veins with a thickness lower than 0.1 mm in the rock matrix. The inhibition of nucleation of new veins, and localizing growth to the backbone veins, as a positive feedback mechanism (Clarks et al., 1995), could then help explain the distribution and sizes of the gypsum veins exposed in the study area.

5.3 Conceptual model

Based on the field observations, vein attributes and our interpretations, a conceptual model is proposed to explain the progressive evolution of an anastomosing vein (or an opening-mode fracture) network (Fig. 9). Initially, a large number of small, isolated veins were generated. Later, coalescence of neighbouring veins, especially sub-parallel en echelon veins, commences during propagation, resulting in the formation of larger veins and a reduction of the population of small veins. Due to the fact that vein growth rate is associated to their sizes (Clarks et al., 1995), nucleation of new fractures and growth of already existing, small veins on either side of large veins are inhibited. Some small veins fall into the stress shadow of large veins nearby and change their direction to be normal to the vein walls (i.e. local σ_1 direction), which later coalesce with the walls. Many veins split into thinner branches during lateral propagation. The linkage of either parallel or oblique, neighbouring veins contributes to the formation of a backbone framework for the transport of minerals. When vein intensity approaches the saturation level, nucleation of new small veins would be inhibited by mechanical interactions of the backbone veins. In this case, the vein arrays should ideally result in a log-normal distribution of vein thickness as opposed to other types of distributions.

6. Conclusions

(1) The thickness distribution of gypsum veins in the Triassic Mercia Mudstone (SW England) is best characterized by a log-normal distribution.

(2) The veins exhibit a size-dependent growth, i.e. positive feedback, where vein growth is largely localized to the largest veins.

(3) Mechanical interaction of vein arrays inhibits nucleation and growth of small veins on either side of large veins, but favours the generation of minor vein branches in tip regions of large veins during their lateral propagation.

(4) Bridging veins contribute to a higher connectivity of a vein network. The mechanical interaction of neighbouring veins would inhibit the nucleation of new veins when vein density approaches a saturation level, which favours a log-normal distribution of vein thickness.

(5) This study suggests that the integrated data of vein (opening-mode fracture) parameters, including thickness and thickness distribution, intersection, volume fraction and fractal distribution, can yield insights into history of progressive evolution of vein networks.

Acknowledgements

This research was funded by Shell International Exploration and Production B.V. We thank Jon Wells for sample preparation and Owen Green for assistance with thin section imaging. Martino Foschi is thanked for fruitful discussions. We appreciate the editorial handling of this paper by Enrique Gomez-Rivas. Reviews by Vincenzo Guerriero and one anonymous reviewer significantly improved the quality of this paper.

References

- Aydin, A., 2000. Fractures, faults, and hydrocarbon entrapment, migration and flow. *Marine and Petroleum Geology* 17, 797-814.
- Bai, T., Pollard, D., Gao, H., 2000. Explanation for fracture spacing in layered materials. *Nature* 403, 753-756.

321 Bai, T., Pollard, D.D., 2000. Fracture spacing in layered rocks: a new explanation based on the
 322 stress transition. *Journal of Structural Geology* 22, 43-57.

323 Berkowitz, B., Bour, O., Davy, P., Odling, N., 2000. Scaling of fracture connectivity in geological
 324 formations. *Geophysical Research Letters* 27, 2061-2064.

325 Bonnet, E., Bour, O., Odling, N.E., Davy, P., Main, I., Cowie, P., Berkowitz, B., 2001. Scaling of
 326 fracture systems in geological media. *Reviews of Geophysics* 39, 347-383.

327 Bons, P.D., Elburg, M.A., Gomez-Rivas, E., 2012. A review of the formation of tectonic veins and
 328 their microstructures. *Journal of Structural Geology* 43, 33-62.

329 Brooks, M., Trayner, P., Trimble, T., 1988. Mesozoic reactivation of Variscan thrusting in the
 330 Bristol Channel area, UK. *Journal of the Geological Society* 145, 439-444.

331 Chandler, F., 1988. Diagenesis of sabkha-related, sulphate nodules in the early Proterozoic Gordon
 332 Lake Formation, Ontario, Canada. *Carbonates and Evaporites* 3, 75-94.

333 Cladouhos, T.T., Marrett, R., 1996. Are fault growth and linkage models consistent with power-
 334 law distributions of fault lengths? *Journal of Structural Geology* 18, 281-293.

335 Clark, M.B., Brantley, S.L., Fisher, D.M., 1995. Power-law vein-thickness distributions and
 336 positive feedback in vein growth. *Geology* 23, 975-978.

337 Cobbold, P.R., Zanella, A., Rodrigues, N., Løseth, H., 2013. Bedding-parallel fibrous veins (beef
 338 and cone-in-cone): Worldwide occurrence and possible significance in terms of fluid
 339 overpressure, hydrocarbon generation and mineralization. *Marine and Petroleum*
 340 *Geology* 43, 1-20.

341 Cosgrove, J.W., 2001. Hydraulic fracturing during the formation and deformation of a basin: A
 342 factor in the dewatering of low-permeability sediments. *AAPG Bulletin* 85, 737-748.

343 Cowie, P.A., Vanneste, C., Sornette, D., 1993. Statistical physics model for the spatiotemporal
 344 evolution of faults. *Journal of Geophysical Research: Solid Earth* 98, 21809-21821.
 345 Curtis, J.B., 2002. Fractured shale-gas systems. *AAPG Bulletin* 86, 1921-1938.
 346 Darcel, C., Bour, O., Davy, P., De Dreuzay, J., 2003. Connectivity properties of two-dimensional
 347 fracture networks with stochastic fractal correlation. *Water Resources Research* 39,
 348 doi:10.1029/2002WR001628.
 349 Dart, C.J., McClay, K., Hollings, P.N., 1995. 3D analysis of inverted extensional fault systems,
 350 southern Bristol Channel basin, UK. *Geological Society, London, Special Publications*
 351 88, 393-413.
 352 Davy, P., Le Goc, R., Darcel, C., Bour, O., De Dreuzay, J.-R., Munier, R., 2010. A likely universal
 353 model of fracture scaling and its consequence for crustal hydromechanics. *Journal of*
 354 *Geophysical Research: Solid Earth* 115, doi: 10.1029/2009JB007043.
 355 Dewhurst, D.N., Yang, Y., Aplin, A.C., 1999. Permeability and fluid flow in natural mudstones.
 356 *Geological Society, London, Special Publications* 158, 23-43.
 357 Einstein, H.H., Baecher, G.B., 1983. Probabilistic and statistical methods in engineering geology.
 358 *Rock Mechanics and Rock Engineering* 16, 39-72.
 359 Engelder, T., Lash, G.G., Uzcátegui, R.S., 2009. Joint sets that enhance production from Middle
 360 and Upper Devonian gas shales of the Appalachian Basin. *AAPG Bulletin* 93, 857-889.
 361 French, M., Boutt, D., Goodwin, L., 2012. Sample dilation and fracture in response to high pore
 362 fluid pressure and strain rate in quartz-rich sandstone and siltstone. *Journal of*
 363 *Geophysical Research: Solid Earth* 117, doi: 10.1029/2011JB008707.
 364 Gale, J.F., Lander, R.H., Reed, R.M., Laubach, S.E., 2010. Modeling fracture porosity evolution
 365 in dolostone. *Journal of Structural Geology* 32, 1201-1211.

366 Gale, J.F., Laubach, S.E., Olson, J.E., Eichhubl, P., Fall, A., 2014. Natural fractures in shale: A
367 review and new observations. AAPG Bulletin 98, 2165-2216.

368 Gale, J.F., Reed, R.M., Holder, J., 2007. Natural fractures in the Barnett Shale and their importance
369 for hydraulic fracture treatments. AAPG Bulletin 91, 603-622.

370 Ghosh, K., Mitra, S., 2009. Two-dimensional simulation of controls of fracture parameters on
371 fracture connectivity. AAPG Bulletin 93, 1517-1533.

372 Gillespie, P., Howard, C., Walsh, J., Watterson, J., 1993. Measurement and characterisation of
373 spatial distributions of fractures. Tectonophysics 226, 113-141.

374 Glen, R., Hancock, P., Whittaker, A., 2005. Basin inversion by distributed deformation: the
375 southern margin of the Bristol Channel Basin, England. Journal of Structural Geology 27,
376 2113-2134.

377 Gudmundsson, A., 1987. Tectonics of the Thingvellir fissure swarm, SW Iceland. Journal of
378 Structural Geology 9, 61-69.

379 Guerriero, V., Iannace, A., Mazzoli, S., Parente, M., Vitale,
380 S., & Giorgioni, M., 2010. Quantifying uncertainties in multi-scale studies of fractured
381 reservoir analogues: Implemented statistical analysis of scan line data from carbonate
382 rocks. Journal of Structural Geology 32, 1271-1278.

383 Guerriero, V., Vitale, S., Ciarcia, S., Mazzoli, S., 2011. Improved statistical multi-scale analysis
384 of fractured reservoir analogues. Tectonophysics 504, 14-24.

385 Guerriero, V., Mazzoli, S., Iannace, A., Vitale, S., Carravetta, A., Strauss, C., 2013. A permeability
386 model for naturally fractured carbonate reservoirs. Marine and Petroleum Geology 40,
387 115-134.

388 Hedenquist, J.W., Lowenstern, J.B., 1994. The role of magmas in the formation of hydrothermal
ore deposits. Nature 370, 519-527.

389 Hobbs, P., Hallam, J., Forster, A., Entwisle, D., Jones, L., Cripps, A., Northmore, K., Self, S.,
390 Meakin, J., 2002. Engineering geology of British rocks and soils: Mudstones of the
391 Mercia Mudstone Group. British Geological Survey, Research report RR/01/02.

392 Hood, S.D., Nelson, C.S., Kamp, P.J., 2003. Modification of fracture porosity by multiphase vein
393 mineralization in an Oligocene nontropical carbonate reservoir, Taranaki Basin, New
394 Zealand. AAPG Bulletin 87, 1575-1597.

395 Hooker, J., Gale, J., Gomez, L., Laubach, S., Marrett, R., Reed, R., 2009. Aperture-size scaling
396 variations in a low-strain opening-mode fracture set, Cozzette Sandstone, Colorado.
397 Journal of Structural Geology 31, 707-718.

398 Hooker, J., Gomez, L., Laubach, S., Gale, J., Marrett, R., 2012. Effects of diagenesis (cement
399 precipitation) during fracture opening on fracture aperture-size scaling in carbonate rocks.
400 Geological Society, London, Special Publications 370, 187-206.

401 Hooker, J., Laubach, S., Marrett, R., 2013. Fracture-aperture size—frequency, spatial distribution,
402 and growth processes in strata-bounded and non-strata-bounded fractures, Cambrian
403 Mesón Group, NW Argentina. Journal of Structural Geology 54, 54-71.

404 Hooker, J., Laubach, S., Marrett, R., 2014. A universal power-law scaling exponent for fracture
405 apertures in sandstones. Geological Society of America Bulletin 126, 1340-1362.

406 Hooker, J.N., Katz, R.F., 2015. Vein spacing in extending, layered rock: The effect of
407 synkinematic cementation. American Journal of Science 315, 557-588.

408 Hooker, J.N., Cartwright, J., Stephenson, B., Silver, C.R., Dickson, A.J., Hsieh, Y.-T., 2016. Fluid
409 evolution in fracturing black shales, Appalachian Basin. AAPG Bulletin 101, 1203-1238.

410 Hooker, J., Laubach, S., Marrett, R., 2018. Microfracture spacing distributions and the evolution
411 of fracture patterns in sandstones. Journal of Structural Geology, 108: 66-79.

412 Howard, A., Warrington, G., Ambrose, K., Rees, J., 2008. A formational framework for the Mercia
 413 Mudstone Group (Triassic) of England and Wales. British Geological Survey, Research
 414 report RR/08/04.

415 Ingraffea, A.R., 1987. Theory of crack initiation and propagation in rock. *Fracture Mechanics of*
 416 *Rock* 10, 93-94.

417 Jafari, A., Babadagli, T., 2011. Effective fracture network permeability of geothermal reservoirs.
 418 *Geothermics* 40, 25-38.

419 Karperien, A., 2013. FracLac for ImageJ. US National Institutes of Health.
 420 <https://imagej.nih.gov/ij/plugins/fraclac/FLHelp/Introduction.htm>.

421 Kasprzyk, A., 1995. Gypsum-to-anhydrite transition in the Miocene of southern Poland. *Journal*
 422 *of Sedimentary Research* 65, 348-357.

423 Kelly, P., Peacock, D., Sanderson, D., McGurk, A., 1999. Selective reverse-reactivation of normal
 424 faults, and deformation around reverse-reactivated faults in the Mesozoic of the Somerset
 425 coast. *Journal of Structural Geology* 21, 493-509.

426 Laubach, S., Reed, R., Olson, J., Lander, R., Bonnell, L., 2004. Coevolution of crack-seal texture
 427 and fracture porosity in sedimentary rocks: Cathodoluminescence observations of
 428 regional fractures. *Journal of Structural Geology* 26, 967-982.

429 Marrett, R., Allmendinger, R.W., 1992. Amount of extension on "small" faults: An example from
 430 the Viking graben. *Geology* 20, 47-50.

431 Mauldon, M., Dunne, W., Rohrbaugh, M., 2001. Circular scanlines and circular windows: new
 432 tools for characterizing the geometry of fracture traces. *Journal of Structural Geology* 23,
 433 247-258.

434 McCaffrey, K., Johnston, J., 1996. Fractal analysis of a mineralised vein deposit: Curraghinalt
435 gold deposit, County Tyrone. *Mineralium Deposita* 31, 52-58.

436 Miliorizos, M., Ruffell, A., 1998. Kinematics of the Watchet-Cothelstone-Hatch fault system:
437 implications for the fault history of the Wessex basin and adjacent areas. *Geological*
438 *Society, London, Special Publications* 133, 311-330.

439 Meng, Q., Hooker, J., Cartwright, J., 2017a. Early overpressuring in organic-rich shales during
440 burial: evidence from fibrous calcite veins in the Lower Jurassic Shales-with-Beef
441 Member in the Wessex Basin, UK. *Journal of the Geological Society* 174, 869-882.

442 Meng, Q., Hooker, J., Cartwright, J., 2017b. Genesis of natural hydraulic fractures as an indicator
443 of basin inversion. *Journal of Structural Geology* 102, 1-20.

444 Meng, Q., Hooker, J., Cartwright, J., 2017c. Lithological control on fracture cementation in the
445 Keuper Marl (Triassic), north Somerset, UK. *Geological Magazine*, 1-15,
446 <https://doi.org/10.1017/S001675681700070X>.

447 Meng, Q., Hooker, J., Cartwright, J., 2018. Role of pressure solution in the formation of bedding-
448 parallel calcite veins in an immature shale (Cretaceous, southern UK). *Geological*
449 *Magazine*, 1-17, <https://doi.org/10.1017/S0016756818000377>.

450 Narr, W., Currie, J.B., 1982. Origin of fracture porosity--example from Altamont Field, Utah.
451 *AAPG Bulletin* 66, 1231-1247.

452 Narr, W., Suppe, J., 1991. Joint spacing in sedimentary rocks. *Journal of Structural Geology* 13,
453 1037-1048.

454 Odling, N., Gillespie, P., Bourguine, B., Castaing, C., Chiles, J., Christensen, N., Fillion, E., Genter,
455 A., Olsen, C., Thrane, L., 1999. Variations in fracture system geometry and their

456 implications for fluid flow in fractured hydrocarbon reservoirs. *Petroleum Geoscience* 5,
457 373-384.

458 Oliver, N.H., Bons, P.D., 2001. Mechanisms of fluid flow and fluid–rock interaction in fossil
459 metamorphic hydrothermal systems inferred from vein–wallrock patterns, geometry and
460 microstructure. *Geofluids* 1, 137-162.

461 Olson, J., Pollard, D.D., 1989. Inferring paleostresses from natural fracture patterns: A new method.
462 *Geology* 17, 345-348.

463 Olson, J.E., 1993. Joint pattern development: Effects of subcritical crack growth and mechanical
464 crack interaction. *Journal of Geophysical Research: Solid Earth* 98, 12251-12265.

465 Olson, J.E., 2003. Sublinear scaling of fracture aperture versus length: An exception or the rule?
466 *Journal of Geophysical Research: Solid Earth* 108, doi: 10.1029/2001JB000419.

467 Ortega, O.J., Marrett, R.A., Laubach, S.E., 2006. A scale-independent approach to fracture
468 intensity and average spacing measurement. *AAPG Bulletin* 90, 193-208.

469 Passchier, C.W., Trouw, R.A., 1996. *Microtectonics*. Springer, Berlin.

470 Philipp, S.L., 2008. Geometry and formation of gypsum veins in mudstones at Watchet, Somerset,
471 SW England. *Geological Magazine* 145, 831-844.

472 Priest, S., Hudson, J., 1976. Discontinuity spacings in rock. *International Journal of Rock*
473 *Mechanics and Mining Sciences & Geomechanics Abstracts* 13, 135-148.

474 Renshaw, C.E., Harvey, C.F., 1994. Propagation velocity of a natural hydraulic fracture in a
475 poroelastic medium. *Journal of Geophysical Research: Solid Earth* 99, 21667-21677.

476 Renshaw, C.E., Pollard, D.D., 1994. Numerical simulation of fracture set formation: A fracture
477 mechanics model consistent with experimental observations. *Journal of Geophysical*
478 *Research: Solid Earth* 99, 9359-9372.

479 Rives, T., Razack, M., Petit, J.-P., Rawnsley, K., 1992. Joint spacing: analogue and numerical
480 simulations. *Journal of Structural Geology* 14, 925-937.

481 Roberts, S., Sanderson, D., Gumiel, P., 1998. Fractal analysis of Sn-W mineralization from central
482 Iberia; insights into the role of fracture connectivity in the formation of an ore deposit.
483 *Economic Geology* 93, 360-365.

484 Roberts, S., Sanderson, D., Gumiel, P., 1999. Fractal analysis and percolation properties of veins.
485 *Geological Society, London, Special Publications* 155, 7-16.

486 Rohrbaugh Jr, M., Dunne, W., Mauldon, M., 2002. Estimating fracture trace intensity, density, and
487 mean length using circular scan lines and windows. *AAPG Bulletin* 86, 2089-2104.

488 Sanderson, D.J., Roberts, S., Gumiel, P., 1994. A fractal relationship between vein thickness and
489 gold grade in drill core from La Codosera, Spain. *Economic Geology* 89, 168-173.

490 Segall, P., Pollard, D.D., 1983. Joint formation in granitic rock of the Sierra Nevada. *Geological*
491 *Society of America Bulletin* 94, 563-575.

492 Shearman, D., Fuller, J., 1969. Anhydrite diagenesis, calcitization, and organic laminites,
493 Winnipegosis formation, Middle Devonian, Saskatchewan. *Bulletin of Canadian*
494 *Petroleum Geology* 17, 496-525.

495 Shearman, D., Mossop, G., Dunsmore, H., Martin, M., 1972. Origin of gypsum veins by hydraulic
496 fracture. *Trans. Inst. Min. Metall.* 81, 149-155.

497 Taylor, S., 1983. A stable isotope study of the Mercia Mudstones (Keuper Marl) and associated
498 sulphate horizons in the English Midlands. *Sedimentology* 30, 11-31.

499 Van Hoorn, B., 1987. The south Celtic Sea/Bristol Channel Basin: origin, deformation and
500 inversion history. *Tectonophysics* 137, 309-319, 323-334.

Walsh, J., Watterson, J., 1993. Fractal analysis of fracture patterns using the standard box-counting technique: valid and invalid methodologies. *Journal of structural Geology* 15, 1509-1512.

Warrington, G., Ivimey-Cook, H., 1992. Triassic. Geological Society, London, Memoirs 13, 97-106.

Weertman, J., Lin, I.-H., Thomson, R., 1983. Double slip plane crack model. *Acta Metallurgica* 31, 473-482.

Figure captions

Fig. 1 Geological map of the study area, southwest UK (left), and distribution of the Mercia Mudstone in the UK (right). Modified from Hobbs et al. (2002) and Hounslow et al. (2004).

Fig. 2 Scatter plot of vein orientation versus vein thickness. N=643.

Fig. 3 Log-log plot of vein thickness versus normalized cumulative frequency.

Fig. 4 (A) Photomicrograph showing a thin elongate-fibrous gypsum vein in red marls. The enlarged box area shows a needle-like gypsum lath. Cross-polarized light. (B) Photomicrograph showing a thin gypsum vein close to two larger veins. Cross-polarized light. (C) SEM-EDS image showing scattered lenticular gypsum laths in the host rock matrix. C, clay. D, dolomite. L, lath. Q, quartz.

524

525 Fig. 5 Outcrop photographs showing sub-horizontal gypsum veins in the red marls exposed in the
526 study area. (A) An isolated sub-horizontal gypsum vein with a maximum thickness of 7.0 cm. Note
527 the absence of gypsum veins in both the upper and lower horizons of this vein. Camera cap is 5.2
528 cm in diameter. (B) Three closely-spaced gypsum veins with significantly varied thickness. The
529 enlarged area shows the smallest vein with a thickness of only 0.06 cm. (C) Multiple sub-parallel,
530 thick gypsum veins. Note that steeply dipping veins are rarely developed within the intervals
531 between neighbouring sub-horizontal veins. Tape measure is 40 cm long.

532

533 Fig. 6 Outcrop photographs showing intersections of gypsum veins. (A) A set of closely spaced en
534 echelon veins. Note the identifiable tapering vein tips. (B) Linkage of a sub-horizontal vein and
535 inclined veins. The sub-horizontal vein split into two branches during propagation. The arrows
536 mark the propagation direction of the veins as indicated by the decreased thickness. (C) An
537 anastomosing gypsum vein network within a 10 cm interval, consisting of predominant gently-
538 dipping veins. Note that the veins frequently curved to link with neighbouring veins. (D) A steeply
539 dipping, bridging gypsum vein linking two neighbouring sub-horizontal veins. (E) Gypsum vein
540 arrays with varied thicknesses and propagation directions (highlighted by arrows). Note that the
541 small veins commonly propagate towards walls of large veins nearby. (F) Multiple veins splitting
542 into thinner branches during propagating towards walls of neighbouring, thicker gypsum veins.
543 The vein branches commonly coalesce with the large vein at approximately 90°.

544

545 Fig. 7 Examples of image analysis of vein networks. (A) and (D) Outcrop photographs showing
546 white gypsum vein networks in red marls. The circles show localities of vein intersections. (B) and

(E) Binary images showing gypsum veins (black) shown in Fig. 7A and 7D respectively. Grid lines are shown to highlight the boxes that contain vein segments. Note that steeply dipping vein are more abundant in Fig. 7D than 7B. (C) and (F) Plot of $\ln \varepsilon$ versus $\ln N(\varepsilon)$ with the data derived from Fig. 7B and 7D respectively.

Fig. 8 (A) Scatter plot of fracture porosity versus fractal dimension versus the number of intersection points of the images analyzed. (B) Scatter plot of fractal dimension versus the number of intersection points, which exhibits a rather positive correlation.

Fig. 9 A conceptual model for progressive evolution of a vein network that would exhibit a log-normal distribution of vein thickness at the final stage. T1: Generation of numerous, isolated veins. T2: Linkage of adjacent veins as they propagate. T3: Localized growth of gypsum to the largest veins following a positive-feedback growth mechanism. Note that generation of new veins is inhibited at this stage.

Table 1. Statistics of goodness-of-fit of the distribution of vein thickness.

Number	Size distribution χ^2 error ^a			
	Power law	Exponential	Normal	Log-normal
a	17.444	16.840	1.904E+09	0.295
b	7.953	13.798	3.814E+07	0.357
c	6.128	3.213	673.651	0.359
d	2.155	3.049	509.065	0.609
e	10.857	2.752	2.060E+04	0.931
f	4.058	1.509	94.079	0.462
g	1.889	3.495	373.312	0.806

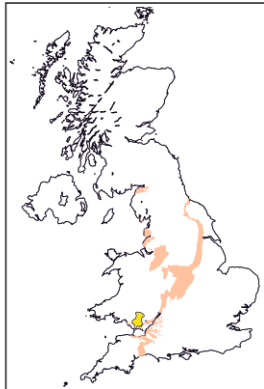
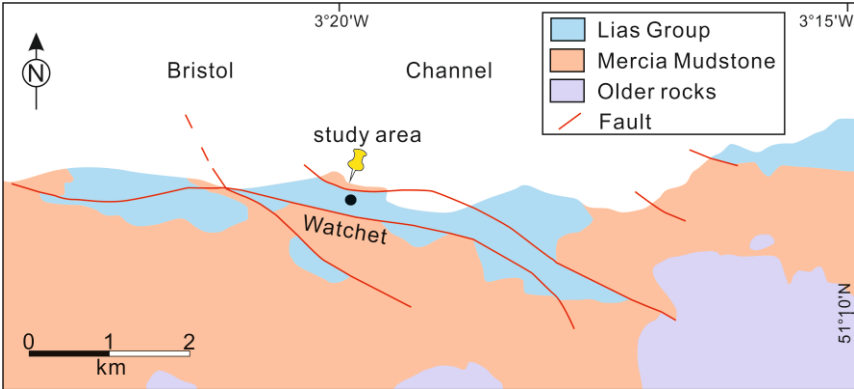
^a Lowest χ^2 error value best fit the distribution.

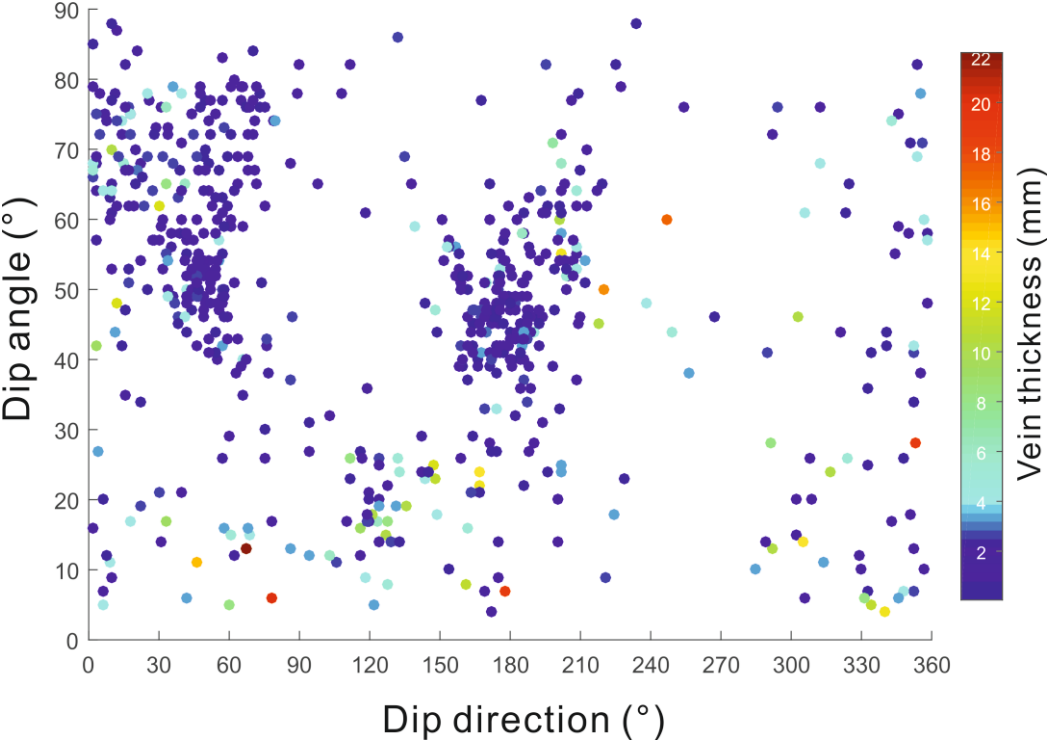
^b The number corresponds to a - g in Fig. 3.

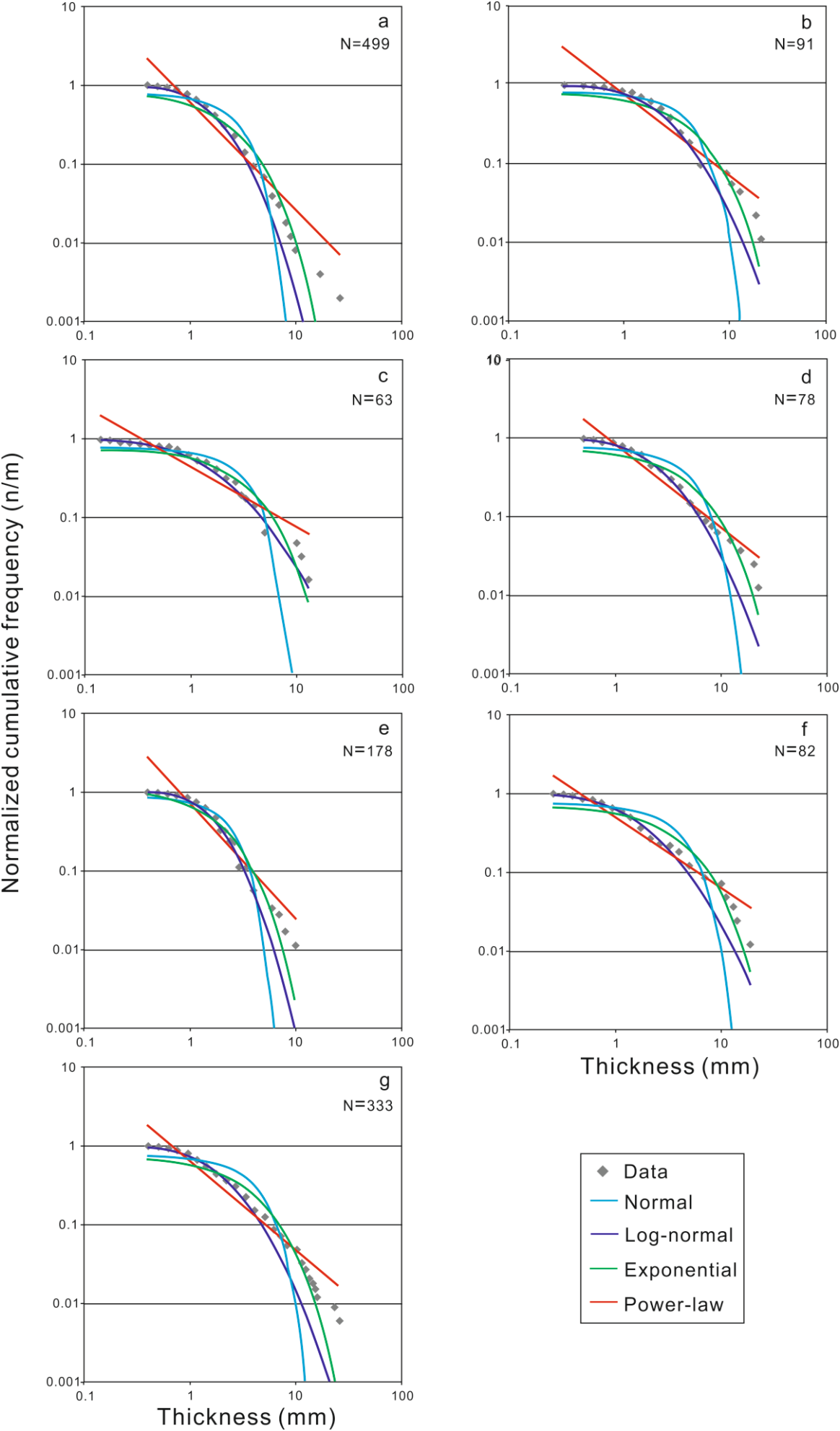
Table 2. Attributes of gypsum veins derived by image analysis.

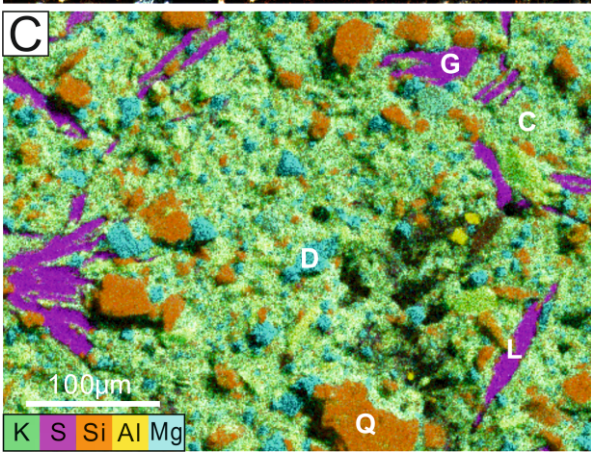
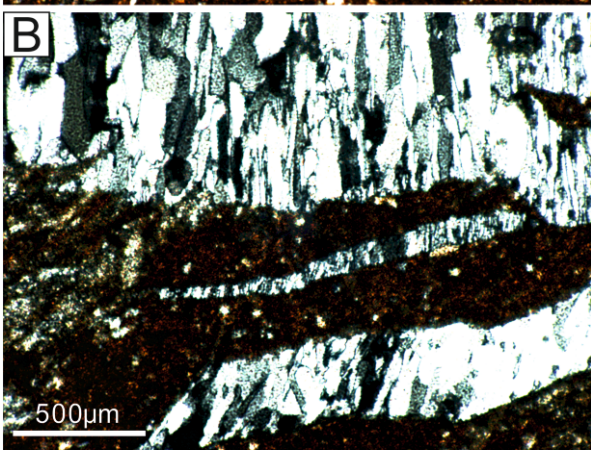
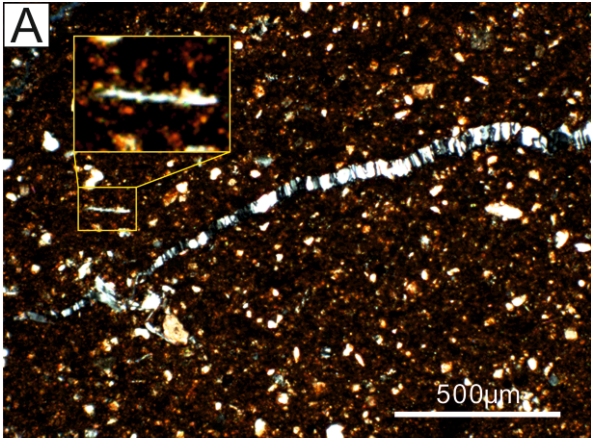
Number ^a	Number of intersection points	Fractal dimension		Vein volume fraction (%)
		'D'	Coefficient of determination, r^2	
1	139	1.5801	0.9905	11.00
2	244	1.6677	0.9910	11.32
3	297	1.6927	0.9900	10.65
4	198	1.6584	0.9893	8.80
5	126	1.5660	0.9934	10.07
6	58	1.4566	0.9884	7.14
7	255	1.6226	0.9906	8.00
8	224	1.6233	0.9905	7.32
9	85	1.4455	0.9877	9.54
10	202	1.6195	0.9923	10.87
11	136	1.5077	0.9904	6.75
12	190	1.6776	0.9921	13.49
13	216	1.5872	0.9950	12.87
14	260	1.6488	0.9930	15.53
15	196	1.6197	0.9934	13.25
16	205	1.7197	0.9949	17.94
17	188	1.6641	0.9937	10.73
18	290	1.7183	0.9943	16.07
19	324	1.6847	0.9925	13.21
20	186	1.6494	0.9926	12.58
21	176	1.6339	0.9911	12.51
22	156	1.6668	0.9909	11.86
23	68	1.5327	0.9935	10.34
24	92	1.5681	0.9903	8.01

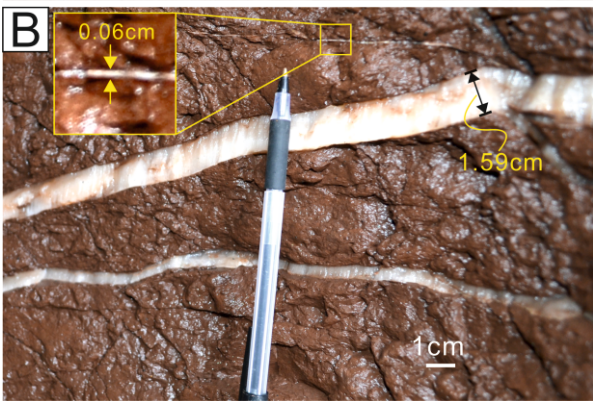
^a the number corresponds to the order of figures provided in the supplementary material.

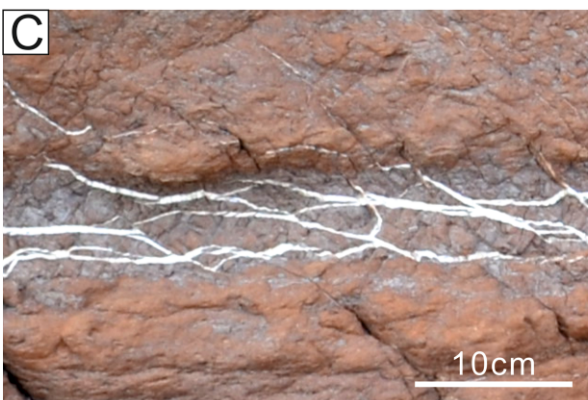
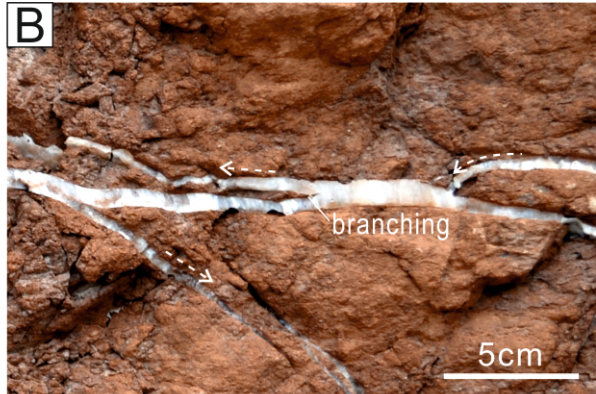


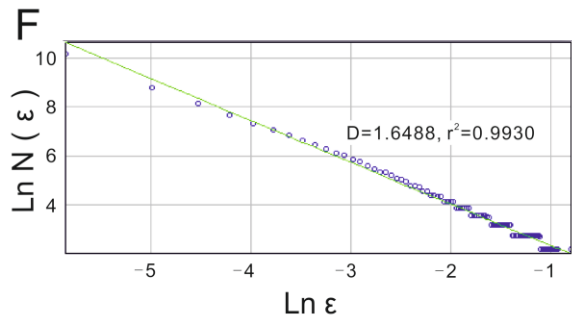
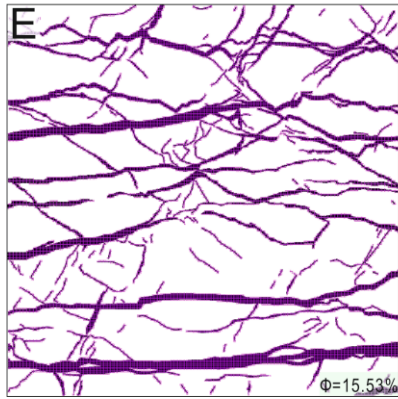
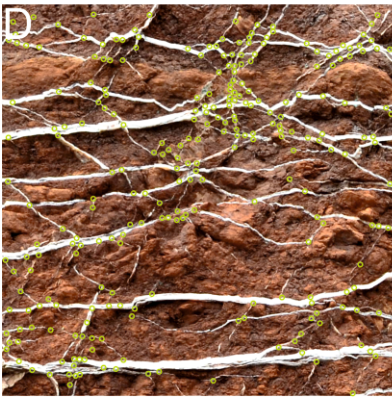
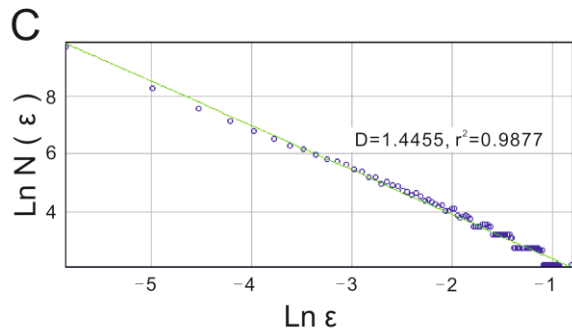
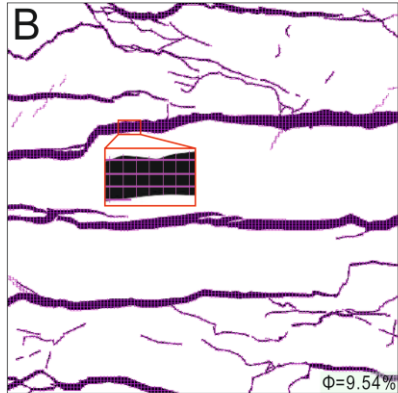
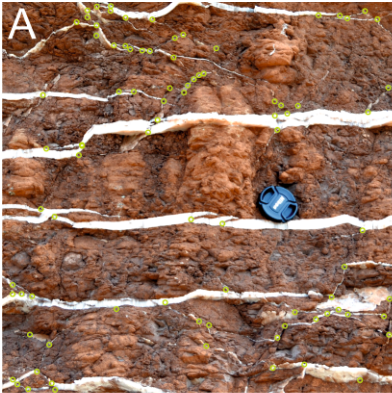


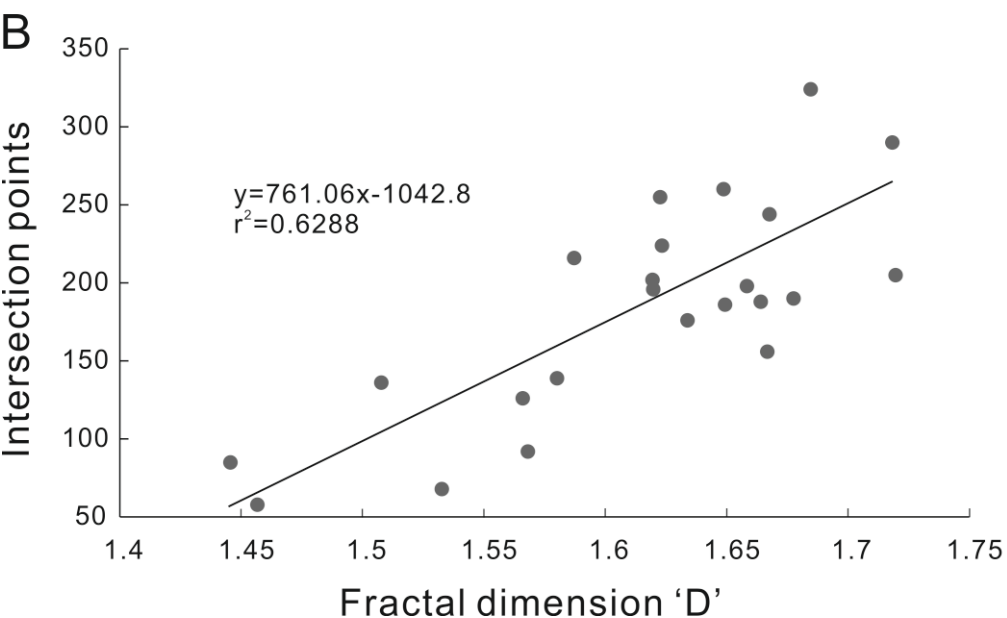
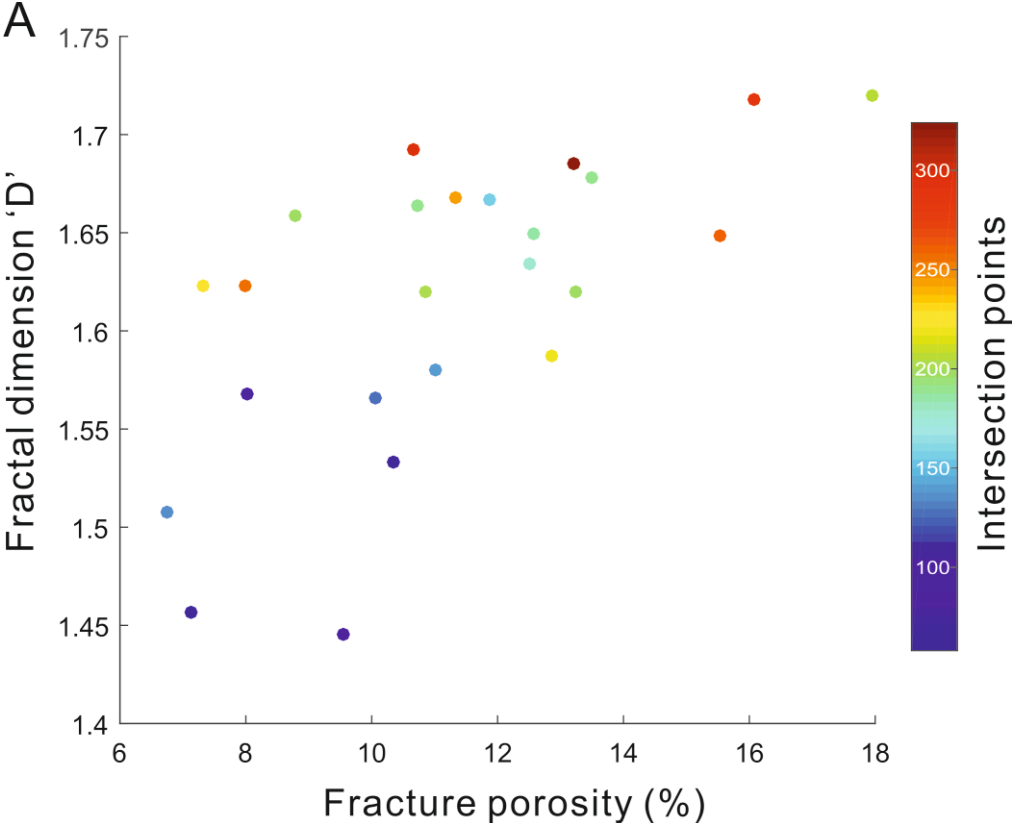




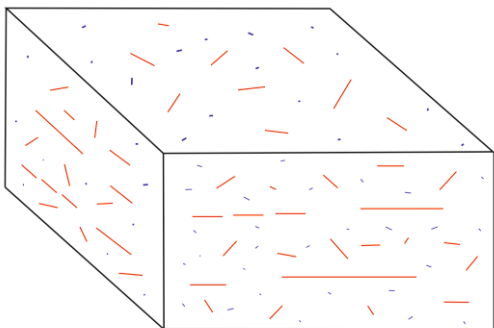




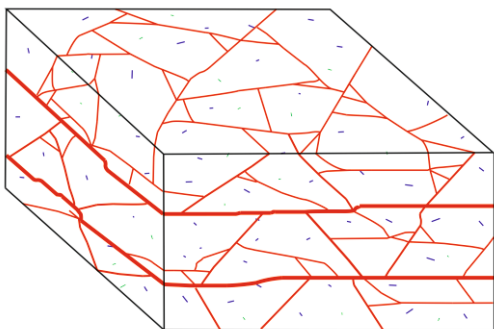




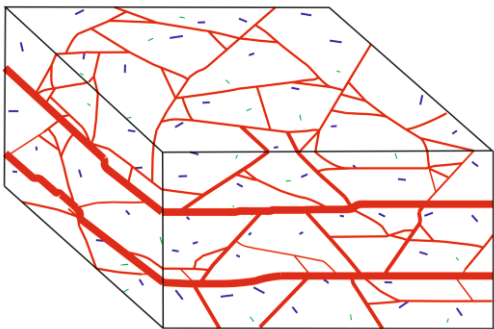
T1



T2



T3



- Backbone veins
- Isolated veins with identifiable tips
- Newly generated veins during T2

Supplementary material

Field photos (left) and their binary images (right) showing gypsum veins.

